Magnetically Actuated Lamina Emergent Mechanism for Bimodal Crawling and Flipping Locomotion

Catherine Jiayi Cai ⓘ, Bok Seng Yeow ⓘ, *Graduate Student Member, IEEE*, Hui Huang ⓘ, Cecilia Laschi ⓘ *, Fellow, IEEE*, and Hongliang Ren ⓘ *, Senior Member, IEEE*

***Abstract*—Magnetically actuated elastomeric soft robots are capable of untethered multimodal locomotion due to their ability to adapt to environments. However, they are usually fabricated with soft materials and suffer from structural instabilities under external loads. We designed a multilayer lamina emergent mechanism (LEM) that is capable of crawling and flipping due to its highly coupled kinematics that enables the simplification of multiple joint control. Each LEM layer is designed as a parallelogram linkage that couples four legs arranged in a staggered manner, giving rise to an alternative tetrapod crawling gait with just two degrees of freedom under the influence of a changing magnetic field. The mechanism is capable of controlled flipping without the need for additional actuators or structural components. The mechanism can crawl at a speed of ∼4.5 mm/s (0.1125 body length/s) when actuated at a frequency of 1.0 Hz. It can flip at a speed of ∼60.4 mm/s (1.5 body length/s) when actuated at a frequency of 0.5 Hz. We demonstrated the potential benefits of multimodal locomotion, where the mechanism can flip to travel faster and overcome obstacles, and crawl for more controlled navigation.

***Index Terms*—Friction-inertia, lamina emergent mechanisms (LEMs), magnetic actuation, multimodal locomotion, origami-inspired robotics.**

Catherine Jiayi Cai is with the Department of Biomedical Engineering, National University of Singapore, Singapore 117580, also with the Department of Electronic Engineering, The Chinese University of Hong Kong, Hong Kong, and also with the Singapore Institute of Manufacturing Technology (SIMTech), Agency for Science, Technology and Research (A∗STAR), Singapore 636732 (e-mail: e000486@u.nus.edu).
Bok Seng Yeow is with the Department of Biomedical Engineering, National University of Singapore, Singapore 117580, and also with the Department of Electronic Engineering, The Chinese University of Hong Kong, Hong Kong (e-mail: e0426370@u.nus.edu).
Hui Huang is with the Singapore Institute of Manufacturing Technology (SIMTech), Agency for Science, Technology and Research (A∗STAR), Singapore 636732, and also with the Singapore Institute of Technology, Singapore 138683 (e-mail: hhuang@simtech.a-star.edu.sg).
Cecilia Laschi is with the Department of Mechanical Engineering, National University of Singapore, Singapore 117575 (e-mail: mpeclc@nus.edu.sg).
Hongliang Ren is with the Department of Electronic Engineering, The Chinese University of Hong Kong, Hong Kong, also with the Department of Biomedical Engineering, National University of Singapore, Singapore 117580, and also with the Department of Electronic Engineering, The Chinese University of Hong Kong, Hong Kong (e-mail: hren@cuhk.edu.hk).
This article has supplementary material provided by the authors and color versions of one or more figures available at https://doi.org/10.1109/TMECH.2023.3297722.
Digital Object Identifier 10.1109/TMECH.2023.3297722

I. INTRODUCTION

MAGNETICALLY actuated soft robots and mechanisms that are capable of untethered multimodal locomotion are attractive due to their ability to access hard-to-reach places [1] by adapting to their environments in a remote and wireless fashion [2]. Several works have reported using magnetic actuation to generate and control different locomotion modes within a single robotic architecture [3], [4], [5]. However, they are commonly fabricated with soft materials. While their low material stiffness allows for easy deformation, they often suffer from structural instabilities under external loads [6], [7], [8]. In contrast to mechanisms that rely on their underlying materials for elastic deformation, soft compliant mechanisms that depend on plastic deformation may provide an alternative method for designing soft robots with a higher degree of resilience [9].

In particular, folding techniques have been employed to design and fabricate compliant mechanisms that can generate motion using actuating magnetic fields [10], [12], [13]. These mechanisms contain many folds that require parallel and coordinated movements of subsets of these folds to constrain the degrees of freedom (DoFs) [14]. To simplify the control associated with actuating these folds, these mechanisms can be designed as integrated mechanisms with highly coupled kinematics and kinetics. Among these, lamina emergent mechanisms (LEMs) are attractive as they are compatible with planar manufacturing techniques and materials and have the potential to demonstrate sophisticated functions with a simple topology [15]. In addition, LEMs are flat foldable, which is beneficial for space saving as they can be stowed compactly during one position of the mechanism's configuration.
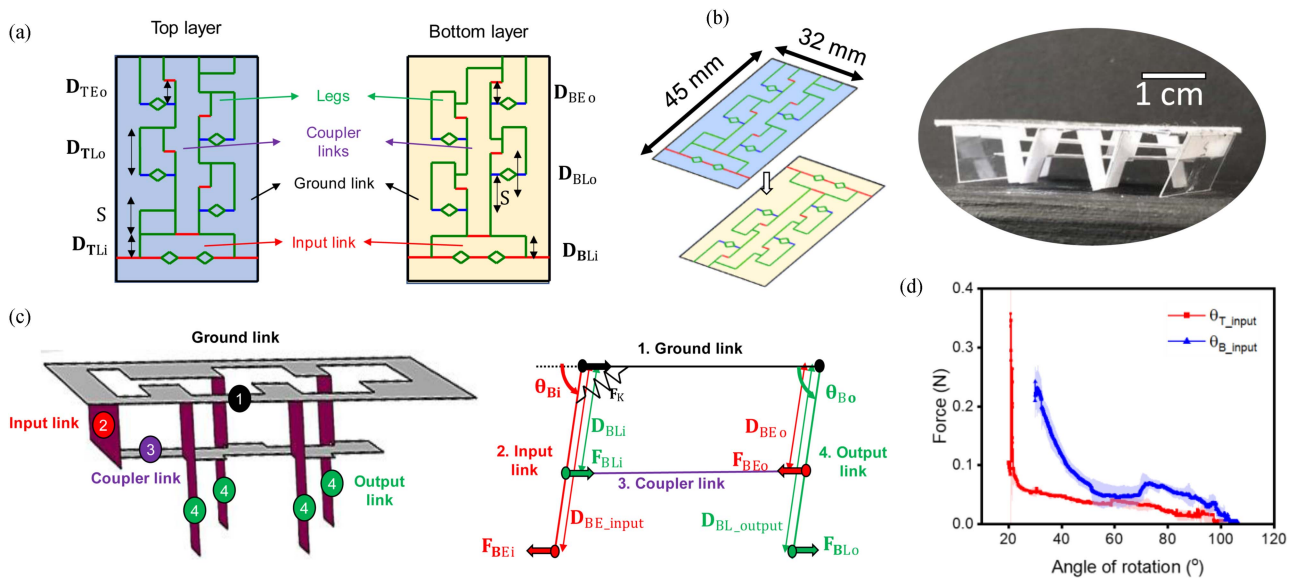
Fig. 1. Design of two LEMs that can be assembled to form a 2-DoF DLEM mechanism. (a) Crease patterns of the two LEM layers. Each layer consists of an input link and four legs coupled by a parallelogram linkage. The crease pattern's red, blue, and green lines represent the mountain folds, valley folds, and cuts, respectively. The folds act as rotational hinge joints. (b) Two LEMs are layered together to form a contact-aided DLEM with eight legs. The blue layer indicates the top LEM layer, while the yellow layer indicates the bottom LEM layer. (c) Kinematics of the parallelogram linkage of the bottom LEM layer. (d) Force characterization of the parallelogram linkage of both LEM layers in the absence of load.

Previously, we designed and fabricated a multilayer LEM (MLEM) as a low DoF mechanism that can be integrated with permanent magnets to crawl under the influence of a magnetic field [16]. However, the prototype had several limitations. First, the prototype was susceptible to slippage and was only able to crawl in confined environments to avoid uncontrollable flipping of the body. Second, the prototype is limited to one mode of locomotion. Finally, the prototype required additional passive feet to create frictional anisotropy to achieve directional movement, rendering the mechanism no longer flat foldable.

In this work, we report a new version of the MLEM prototype that aims to overcome these limitations. The newly designed MLEM employs a more stable crawling gait pattern even under external load and is also capable of controllable flipping to overcome obstacles. The newly designed MLEM does not require passive structures to induce directional motion and retains its flat foldability. The prototype has a dimension of 45 mm × 32 mm × 23 mm (length, width, and height, respectively) and weighs only 2.5 g in total. The main contributions of this work are as follows.

1) Design and assembly of LEMs based on four-bar parallelogram linkages that can give rise to an alternative tetrapod crawling gait.
2) Magnetic actuation of the prototype that gives rise to bimodal crawling and flipping locomotion.
3) Characterization, modeling, and experimental analysis of the prototype's locomotion performance.

II. DESIGN OF DUAL-LAYER LEM (DLEM)

In a single LEM layer, the links and joints lie in the same plane and are, thus, susceptible to a change-point condition when the links become collinear and simultaneously aligned,

allowing unconstrained and undesirable motion. To avoid the change-point state, we stack multiple LEM layers to form an MLEM where one layer contacts another when the mechanism moves. This creates contact-aided behavior to restrict the range of motion (ROM) of the layers, inhibiting them from going into undesirable configurations [17].

A. LEM Design

We designed two LEMs each consisting of an input link and four rectangular legs connected to the planar sheet via valley folds that serve as rotational hinge joints [see Fig. 1(a)]. The four legs and input link are coupled by a parallelogram linkage via a mountain fold. Layering these two LEMs gives rise to an eight-legged DLEM [see Fig. 1(b)]. By rotating the parallelogram linkage of the top LEM layer in the opposite direction as the bottom LEM layer, the legs of each parallelogram linkage will come into contact with each other, restricting the ROM of each LEM such that they do not enter the change-point state.

In our previous work, the legs were arranged in line with each other to give rise to a synchronized gait. However, we found the locomotion to be relatively unstable as the structure was susceptible to uncontrollable flipping in the absence of environmental constraints [16]. Hence, we arranged the legs in a staggered manner, giving rise to an alternative tetrapod crawling gait instead, similar to that observed in arachnids [18].

One advantage of using LEMs lies in their highly coupled nature, which can simplify control of motions and tasks that traditionally require individual control of many DoFs to obtain similar movements in a complex and high-dimensional configuration space [19]. For example, Wang et al. [20] performed a kinematic study of the alternative tetrapod locomotion observed in spiders and found that the system had 94-DOFs when eight legs were in contact with the surface. In contrast, the DLEM

in this work only has 2-DOFs, where each LEM governs one independent DOF.

The folding pattern of each LEM is shown in Fig. 1(a). Each LEM layer has a dimension of 45 mm × 32 mm, where the length of the coupler and input/output links of the top LEM layer is 40 mm and 5 mm, respectively, and 40 mm and 4.5 mm, respectively, for the bottom layer. The length and width of the legs are 10 mm and 5 mm, respectively, with a foot-to-foot spacing (S) of 8 mm.

B. Design Parameters

The main crux of the LEM design lies in the planar four-bar parallelogram linkage that couples the legs together. Each link translates into the base plane and rotates parallel around an axis perpendicular to that plane [2]. The four legs can be modeled together as an output link that can be simultaneously rotated with the input link via the coupler link [see Fig. 1(c)]. The ground link is the base plane where the LEM is anchored. The four-bar linkage can be modeled as two levers (input and output links) connected by a coupler link. The fulcrum is the hinge joint joining the input and output links to the ground link. Rotation of the input and output link is achieved by moments generated by forces exerted due to the effort and load, which is dependent on their respective distances from the pivot.

1) Relative Length of Links: Depending on the desired relationship between the motion of the input and output link, the relative length of the links relative to each other can be modified as per Grashof's condition for four-bar linkages [21]. For this work, we designed the LEMs as parallelogram mechanisms as they enable the transmission of synchronous motion [22] and are flat foldable [23].

2) Mechanical Advantage (MA): The ratio of the output force to the input force of mechanical linkages is known as the MA. In the case of the input link, the load experienced (F_{Li}) is the resistance experienced by the output link as transmitted by the coupler link located at a distance (D_{Li}) from the fulcrum (load arm). Efforts can be exerted on the end of the input link (F_{Ei}) at a distance (D_{Ei}) from the fulcrum such that $D_{Ei} > D_{Li}$. Since the load is located between the effort and the fulcrum, the input link can be modeled as a class two lever where the MA is given as follows:

$$MA = \frac{D_{Ei}}{D_{Li}} > 1. \tag{1}$$

Due to the assembly of the LEMs, the load arm of the input link of the top layer will inevitably be longer than that of the bottom layer ($D_{TLi} > D_{BLi}$), resulting in a smaller MA. For the same given input applied force (F_{Ei}), the input link of the bottom LEM layer is expected to experience greater output force and net moment to undergo a greater angle of rotation as compared with the top LEM layer ($F_{BLi} > F_{TLi}$, $|\theta_{Bi}| > |\theta_{Ti}|$). A benefit of this asymmetry in rotation angle is that it can be used to induce net forward motion such that we can eliminate the need for structures that were previously required in friction-reliant locomotion to induce frictional anisotropy for directional movement [8], [16], [24], [25]. More on this will be elaborated in Section II-E.

However, due to the contact-aided behavior of the assembled DLEM, we do not want the difference in MA of the two LEM layers to be too large, as this will result in a lower transmission of torque via the coupler linkage, such that the torque transmitted may not be sufficient to overcome the friction in the system. The angle of rotation of the output links of the top (θ_{To}) and bottom (θ_{Bo}) LEM is under the following constrain by trigonometry [see Fig. 3(a)]

$$\theta_{Bo} + \theta_{To} = 180° - \sin^{-1}\left(\frac{S\sin\theta_{To}}{D_{ELo}}\right). \tag{2}$$

For a given force in the coupler link, the torque transmitted to the output bar decreases substantially when the transmission angle (θ_o) deviates significantly from 90°. In the case of a parallelogram linkage, it is recommended for the range of angular motion to remain between 50° and 130° to avoid large transmission losses (i.e., $|\theta_i|$, $|\theta_o| > 40°$) [22]. When the MA of the bottom LEM is significantly larger than the top LEM, the angle of rotation of the bottom LEM (θ_{Bo}) risks becoming smaller than 40°.

3) Length of Legs (L) to Foot-to-Foot Spacing (S) Ratio: In the design of LEMs, all the links are coplanar in their initial flat state [26]. As a result, by nature of our current design, S must be greater than the leg length L. According to Lu et al. [6], a smaller L/S ratio is associated with more stable locomotion. While this can be achieved by having a large S, this impacts the contact-aided behavior of the MLEM as each LEM layer can undergo a larger range of rotation before contacting each other. This may also result in greater transmission loss via the coupler link from the input to the output link [refer to (2)]. Due to the above limitations, we use an L/S ratio of 1.25.

4) Material and Geometry: Similar to compliant mechanisms, the stress and flexibility of LEMs can be manipulated by changing the geometry, material properties, or boundary conditions [15]. The general dimension of the mechanism (length, width, and height) depends on the intended function and the working environment. As a proof of concept, we fold a physical prototype using regular A4 paper (80 gsm) as the laminae and reinforce the facets with polystyrene to increase the rigidity of the links. Depending on the requirements of the intended application, other sheet materials, such as graphene [27], [28], polymers [29], [30], and carbon fiber [31], can also be used. As the stiffness of the paper tends to reduce the ROM of the folds, we added diamond cutouts in the valley folds [see Fig. 1(a)] to release the stress concentrations [32].

C. Modeling

The folds in the LEMs are often regarded as a "pseudojoint" as they are compliant and, thus, have certain stiffness [23]. Using the pseudorigid-body model, we can represent each LEM as a pseudorigid body where the facets are modeled as links, and each fold is modeled as 1-DoF revolute joint with a torsional spring that provides a restoring elastic moment with equivalent force-deflection characteristics [21], [33]. Depending on the moment produced by the joint, the effect of the torsional spring may or may not be negligible. To understand the behavior of the

This article has been accepted for inclusion in a future issue of this journal. Content is final as presented, with the exception of pagination.

4   IEEE/ASME TRANSACTIONS ON MECHATRONICS

LEM, we first aim to characterize the relationship between the force/moment exerted on the parallelogram input linkage and its corresponding angle of rotation [see Fig. 1(c)].

In the case of the output link, the load experienced (F_{Lo}) is the friction experienced at the tips of the legs during the crawling locomotion, located at a distance of D_{Lo} from the fulcrum. An effort will be applied by the input link as transmitted by the coupler link (F_{Eo}) at a distance D_{Eo} from the fulcrum such that $D_{Lo} > D_{Eo}$. Since the effort is between the load and the fulcrum, the output link can be modeled as a class three lever. To rotate the output link on a flat planar surface, the minimum moment created by the effort (M_{Eo}) must be large enough to balance or overcome the moment caused by the load (M_{Lo})

$$M_{Eo} - M_{Lo} \geq 0 \tag{3}$$

where $M_{Eo} = \mu m g D_{Eo} \sin^2 \theta_o$ and $M_{Lo} = F_{Lo} D_{Lo} \sin(\theta_o)$. μ is the static coefficient of friction between the LEM and the surface it is interacting with, m is the total mass of the LEM prototype, g is the gravitational constant, and θ_o is the angle of rotation of the output link with respect to the ground link.

The force applied to the output link is transmitted through the coupler link. We assume the force acting in the coupler link to be pure tension or compression with negligible bending action. As per Newton's third law, in an ideal parallelogram linkage with no transmission losses at static equilibrium

$$M_{Li} = M_{Eo}. \tag{4}$$

To rotate the input link on a flat planar surface, the minimum moment created by the effort (M_{Ei}) must be large enough to balance or overcome the moment caused by the load (M_{Li}) and the rotational stiffness (M_k) of the mechanism

$$M_{Ei} - M_{Li} - M_k \geq 0 \tag{5}$$

where $M_{Ei} = F_{Ei} D_{Ei} \sin(\theta_i)$, $M_{Li} = F_{Li} D_{Li} \sin(\theta_i)$, and $M_k = k \Delta \theta_i$. k is the overall stiffness coefficient of the mechanism and θ_i is the angle of rotation of the input link with respect to the ground link.

Fig. 1(d) shows the amount of force required to rotate the input links of both the top and bottom LEM when $M_{Li} = 0$. The force experienced by the input links was measured using a force sensor *F/T* Sensor: Nano17 (ATI Industrial Automation). The motion of the mechanism was captured as a video by a camera at 30 fps and the angle of rotation was tracked using the open-source Physlets Tracker video analysis and modeling tool [34]. Five sets of data were collected and the mean and standard deviation were calculated accordingly.

D. Magnetic Actuation

Magnetic actuation is commonly employed for applications where untethered, fast, and real-time manipulation is desirable. Compared with electromagnets, permanent magnets are usually inexpensive and more available and, hence, widely used as magnetic sources in the literature [6], [35], [36], [37]. However, they tend to produce highly variable and unstable magnetic fields that change dramatically with position [38]. As such, they require accurate magnetic models to implement control strategies to
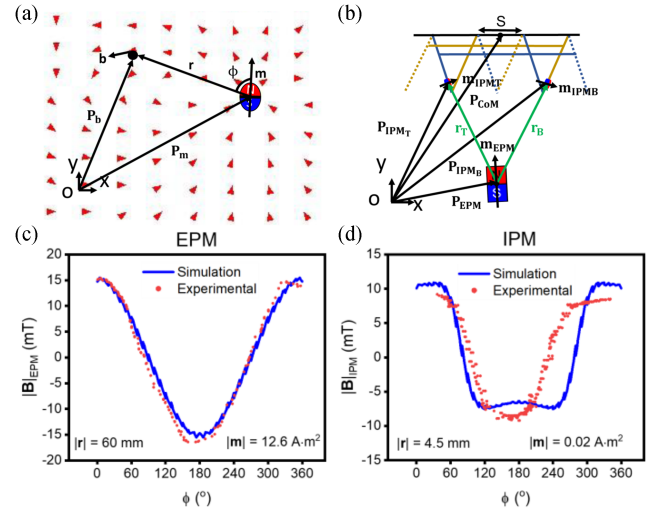

Fig. 2. Characterization of permanent magnets. (a) Representation of magnetic flux density produced by a magnetic dipole. (b) Position and orientation of IPMs on the DLEM and their magnetic interactions with the EPM. Characterization and simulation of the (c) EPM and (d) IPM used in this work.

optimize the orientation and positioning of the magnet for safe and stable interactions.

Fig. 2(a) shows a representation of a magnetic dipole (of magnetic moment **m**) generating magnetic field lines that are radially symmetrical about its magnetization direction. According to Abbott et al. [2], the magnetic flux density **b** generated tangent to the magnetic field lines by a magnetic dipole (located at $\mathbf{P_m}$) on a region of interest (located at $\mathbf{P_b}$) can be approximated by the dipole model as follows:

$$\mathbf{b}\{\mathbf{r}, \mathbf{m}\} = \frac{\mu_0}{4\pi|\mathbf{r}|^3} \left(3\hat{\mathbf{r}}\hat{\mathbf{r}}^T - \mathbf{I}\right)\mathbf{m} \tag{6}$$

where $\mu_0 = 4\pi \times 10^{-7}$ T·m·A^{-1} is the permeability of free space, $\mathbf{r} = \mathbf{P_b} - \mathbf{P_m}$, and **I** is the identity matrix.

In contrast to our previous work where the internal permanent magnets (IPMs) were placed on the legs of the LEM, we chose to attach an IPM on the input link of each LEM layer instead. The IPMs were orientated such that the x-component of their magnetic moments $\mathbf{m_{IPMT}}$ and $\mathbf{m_{IPMB}}$ is aligned, as shown in Fig. 2(b). When we change the relative position and orientation of an external permanent magnet (EPM) with respect to the IPMs, the simultaneous effects of the forces and torques generated by the magnetic field on each IPM can rotate the input link to generate locomotion. In a nonuniform magnetic field, the magnetic force and torque generated by the magnetic field impart tangential forces and moments on the input links (M_{Ei}) to initiate rotation of the input link [refer to (5)]. The force ($\mathbf{f_T}$ and $\mathbf{f_B}$) and torque ($\boldsymbol{\tau_T}$ and $\boldsymbol{\tau_B}$) exerted on the IPMs at locations $\mathbf{P_{IPMT}}$ and $\mathbf{P_{IPMB}}$, respectively, are given by

$$\mathbf{f}_{\boldsymbol{\alpha}} = \frac{3\mu_0}{4\pi|\mathbf{r}_{\boldsymbol{\alpha}}|^4}\left[\left(\widehat{\mathbf{r}_{\boldsymbol{\alpha}}}^T\mathbf{m_{IPM\alpha}}\right)\mathbf{m_{EPM}} + \left(\widehat{\mathbf{r}_{\boldsymbol{\alpha}}}^T\mathbf{m_{EPM}}\right)\mathbf{m_{IPM\alpha}}\right.$$

This article has been accepted for inclusion in a future issue of this journal. Content is final as presented, with the exception of pagination.

CAI et al.: MAGNETICALLY ACTUATED LAMINA EMERGENT MECHANISM FOR BIMODAL CRAWLING AND FLIPPING LOCOMOTION 5
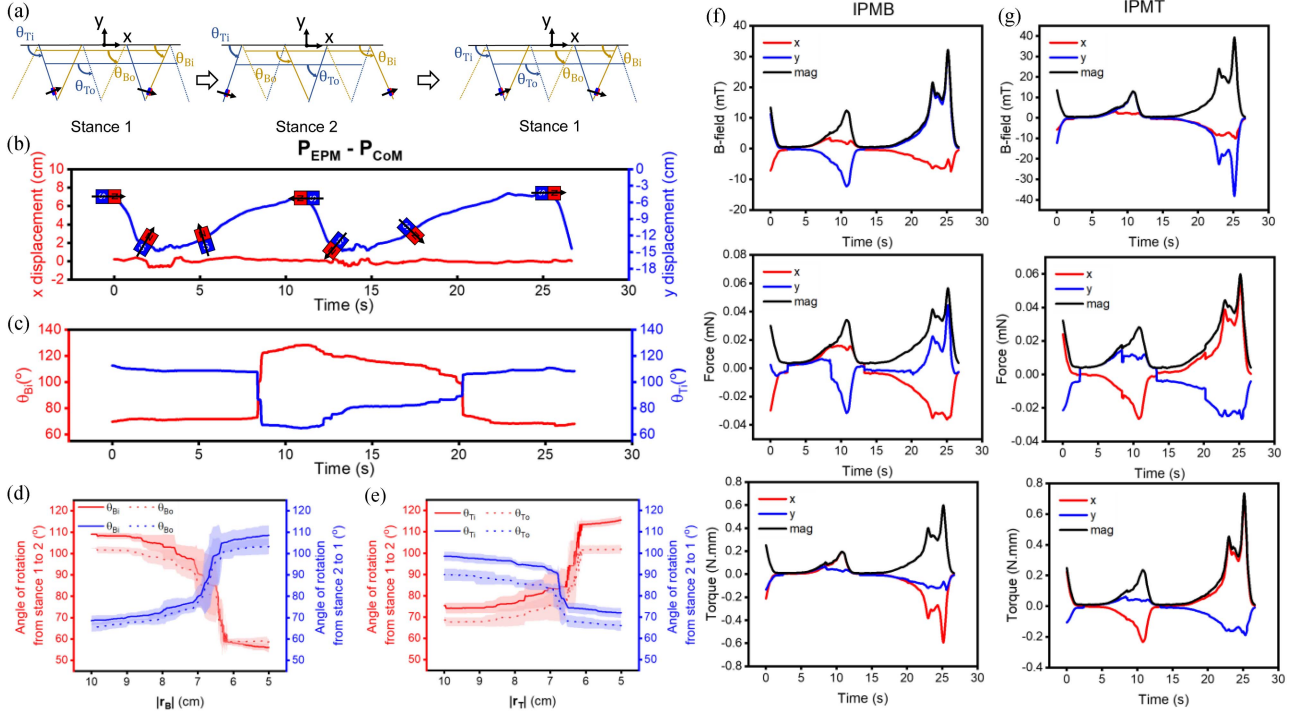

Fig. 3. Magnetic actuation of alternative tetrapod crawling gait in the absence of friction. (a) Mechanism switches between two stances under the influence of a changing magnetic field induced by (b) changing the position and orientation of the EPM along its x-axis. (c) Angle of rotation of the input links of the two LEM layers over time. Relationship between the distance of the EPM and the angle of rotation of the input and output links for the (d) top LEM and (e) bottom LEM layers. Magnetic flux density, force, and torque exerted on the IPMs on the (f) bottom and (g) top layer, respectively.

$$+ \left(\mathbf{m_{EPM}^T m_{IPM\alpha}} - 5 \left(\widehat{\mathbf{r}_\alpha}^T \mathbf{m_{EPM}} \right) \left(\widehat{\mathbf{r}_\alpha}^T \mathbf{m_{IPM\alpha}} \right) \right) \mathbf{r_\alpha} \right] \tag{7}$$

$$\boldsymbol{\tau_\alpha} = \mathbf{S} \{ \mathbf{m_{IPM\alpha}} \} \left[\frac{\mu_0}{4\pi |\mathbf{r_\alpha}|^3} \left(3 \widehat{\mathbf{r}_\alpha} \widehat{\mathbf{r}_\alpha}^T - \mathbf{I} \right) \right] \mathbf{m_{EPM}} \tag{8}$$

where α = T or B for the IPM on the top (IPM_T) and the bottom (IPM_B) LEM layer, respectively, $\mathbf{m_{EPM}}$ is the magnetic moment of the EPM, and $\mathbf{S}\{\mathbf{m_{IPM\alpha}}\}$ is the skew-symmetric matrix packing of a vector used in the cross-product operation.

We use neodymium disc magnets (5 mm × 1 mm) and an N52 neodymium–iron–boron (NdFeB) alloy cube magnet (side 25 mm) from Titan Magnetics as the IPMs and EPM, respectively. The disc magnets were chosen because their flatness enables them to integrate well with the planar and flat-foldable nature of the LEM mechanism [39]. While the diameter of the IPM is arbitrary, we chose the maximum size that could fit onto the input links as a larger magnet is usually associated with greater magnetic flux and, hence, can be actuated using weaker magnetic fields [5]. To get the approximate values of the magnitude of $\mathbf{m_{EPM}}$ and $\mathbf{m_{IPM}}$, we used a magneto-static finite-element solver [40] and approximated the permanent magnet as an inscribed cylinder that is axis symmetric about the axial direction of magnetization. We adjusted the normal coercivity of the simulated magnetic source to match the b-field obtained from calibration experiments where we measured the magnetic flux density of the EPM and IPM at different tilt angles from a fixed distance [see Fig. 2(c) and (d)]. From the

simulation, we estimated the magnitude of $\mathbf{m_{EPM}}$ and $\mathbf{m_{IPM}}$ to be approximately 12.6 A · m² and 0.02 A · m², respectively.

As the IPMs are attached to the input links, they are positioned sufficiently far apart such that the magnetic field generated between the IPMs is negligible throughout the locomotion cycles [41]. The EPM is manually positioned and manipulated to control the direction and strength of the induced magnetic field throughout the actuation of the mechanism. The motion of the mechanism is captured as a video by a camera at 30 fps and the open-source Physlets Tracker video analysis and modeling tool [34] was used to track the x–y coordinate of the EPM, IPMs, center of mass (CoM) of the mechanism, and the angles of rotation of the linkages.

E. Crawling Locomotion

To induce crawling, we position the EPM between the two IPMs and orientate the EPM such that the magnetization direction aligns along the x-axis. When the distance between the EPM and IPMs is sufficiently close, the magnetic field generated by the EPM will be strong enough to induce torque and force on the IPMs, causing a rotation in the input link and, consequently, the legs of each LEM layer. Fig. 3(a)–(e) shows how changing the orientation of the EPM can be used to rotate the legs of the LEM when not in contact with any surfaces ($M_{Li} = 0$). When the x-component of the magnetization direction of the EPM ($\mathbf{m_{EPMx}}$) aligns with that of the magnetization direction of the IPMs ($\mathbf{m_{IPMTx}}$, $\mathbf{m_{IPMBx}}$), the input links of each LEM

TABLE I
PARAMETER VALUES TO INDUCE CHANGE IN STANCES

	Stance 1 to 2		Stance 2 to 1	
	IPMB	IPMT	IPMB	IPMT
$\mathbf{r}$ (cm)	6.29	6.20	6.59	6.71
$\mathbf{|b|}$ (mT)	5.29	4.89	4.85	5.06
$\mathbf{|f|}$ (mN)	0.0166	0.0155	0.0155	0.0178
$\mathbf{|\tau|}$ (N·mm)	0.103	0.0977	0.0938	0.0975

layer rotate toward each other (stance 1). When $\mathbf{m_{EPMx}}$ is in the opposite direction as $\mathbf{m_{IPMTx}}$ and $\mathbf{m_{IPMBx}}$, the input links of each LEM layer will rotate away from each other (stance 2).

From Fig. 3(c)–(e), we observed that the input links of both LEM layers undergo a greater range of rotation when switching from stance 1 to 2 than from stance 2 to 1. We hypothesize that this is due to the rotational stiffness of the hinge joints of the LEM that is present when the links are rotating away from their initial planar state (stance 1 to 2). Hence, when the EPM is brought away from the mechanism when it is in stance 2, the moment induced by the rotational stiffness of the folds causes the input links of each LEM to rotate toward its initial planar state.

From Fig. 3(d) and (e), we observed that even though the angles of rotation of both LEMs are within the range of 50°–130°, nonnegligible transmission losses are still present, as evidenced by the deviation of the transmission angle (θ_{To} and θ_{Bo}) from the input angle (θ_{Ti} and θ_{Bi}). From Fig. 3(d), we observed that the input link of the top LEM layer undergoes a rotation of ~75° to ~115° when switching from stance 1 to 2, and ~100° to ~70° from stance 2 to 1. In contrast, the legs (output link) undergo a rotation of ~70° to ~100° from stance 1 to 2, and ~90° to ~65° from stance 2 to 1. From Fig. 3(e), we observed that the input link of the bottom LEM layer undergoes a rotation of ~110° to ~55° when switching from stance 1 to 2, and ~70° to ~110° from stance 2 to 1. In contrast, the legs undergo a rotation of ~100° to ~60° from stance 1 to 2, and ~65° to ~105° from stance 2 to 1. This corresponds to a deviation angle of $5° - 15°$ for both LEM layers. It is noted that the range of angle of rotation of the top LEM input link (~45°) is smaller than that of the bottom LEM input link (~55°), which supports our earlier analysis where we hypothesized the MA of the bottom LEM layer to be greater than that of the top LEM layer.

From Fig. 3(b) and (c), we observed that, to induce a change in stances from stance 1 to 2 ($t \sim 8.4$ s,) and stance 2 to 1 (20.3 s), the EPM has to be positioned ~7.10 cm away from the center of the robot ($\mathbf{P_{CoM}}$). The corresponding distance of the EPM from the IPM and the simulated magnetic flux density, force, and torque exerted on the IPMs by the EPM is given to 3 significant figures (s. f.) in Table I [see Fig. 3(d)–(g)].

F. Flipping Locomotion

In nature, several animals employ the same limbs for different modes of locomotion [42]. Among these, the *Cebrennus rechenbergi* (cartwheel spider) has been used as inspiration for robots and mechanisms that are capable of flipping and crawling [43], [44], [45], [46], [47], [48]. To realize the flipping motion,

we attach two DLEMs back-to-back to form an MLEM [see Fig. 4(a)]. The DLEMs are assembled in a manner that the bottom input linkage of the second (top) DLEM (DLEM2T) is aligned with that of the top input linkage of the first (bottom) DLEM (DLEM1B) along the y-axis. The position of the bottom input linkage of the top DLEM layer (DLEM2) determines where the head of the robot (the end where the robot flips over) is. The IPMs are oriented such that the x-component of their magnetic moments $\mathbf{m_{IPM2B}}$ and $\mathbf{m_{IPM1T}}$ is in the same direction. The mechanics of the flipping of the mechanism will not be covered in this article, but one can refer to rigid-body rotation, such as that found in [48].

To induce flipping, we position the EPM in front of the mechanism and orientate the EPM such that the magnetization direction $\mathbf{m_{EPM}}$ aligns along the y-axis. When the distance between the EPM and IPMs is sufficiently close, the magnetic field generated by the EPM will be strong enough to induce a torque and force on IPM2B and IPM1T, rotating the IPMs such that their magnetization profile attempts to align with that of the y-axis. This causes the mechanism to tilt and flip over its head [see Fig. 4(b)–(d)].

From Fig. 4(b), we observed that a flipping cycle can be split into five phases as follows:
1) resting;
2) tilting;
3) neutral upright;
4) self-righting;
5) landing.

As the EPM is brought closer to the mechanism, IPMT rotates such that the corresponding input linkage rotates inward toward its initial planar state (θ_{DLEM1T} decreases from ~84° to ~51°), as shown in Fig. 4(d). This causes the mechanism to tilt forward, bringing IPM2B closer to the EPM [see Fig. 4(b)]. When IPM2B is sufficiently close to the EPM, IPM2B will also rotate such that the corresponding input linkage rotates outward and away from its initial planar state (θ_{DLEM2B} increases from ~100° to ~167°), until it can contact the traveling surface such that the mechanism is now upright. As the bottom LEM layer of the top DLEM is able to rotate more than the top LEM layer of the bottom DLEM due to the differences in MA, the mechanism will flip past its neutral y-axis. When the EPM is removed, the mechanism will continue to flip due to the torque induced by the position of its CoM. It is crucial for the MA of the LEM input link of the top DLEM layer to be great enough to generate sufficient rotation under the applied magnetic field for the mechanism to achieve phase 4). When we reverse the direction of the mechanism such that $\mathbf{m_{IPM2T}}$ is at the head of the mechanism, the mechanism is unable to tilt and rotate past its neutral axis and is, hence, unable to flip over its head. Given that the dipole moments of the IPMs are now facing the opposite direction, the y-direction of the magnetic dipole of the EPM will also have to be reversed to continue flipping the mechanism.

We observed that to induce the mechanism to flip (~0.7 s), the EPM has to be ~4.14 cm away from the center of the robot [see Fig. 4(c)]. The corresponding simulated magnetic flux density, force, and torque exerted on the IPMs by the EPM is given to 3 s. f. in Table II [see Fig. 3(e) and (f)].

This article has been accepted for inclusion in a future issue of this journal. Content is final as presented, with the exception of pagination.

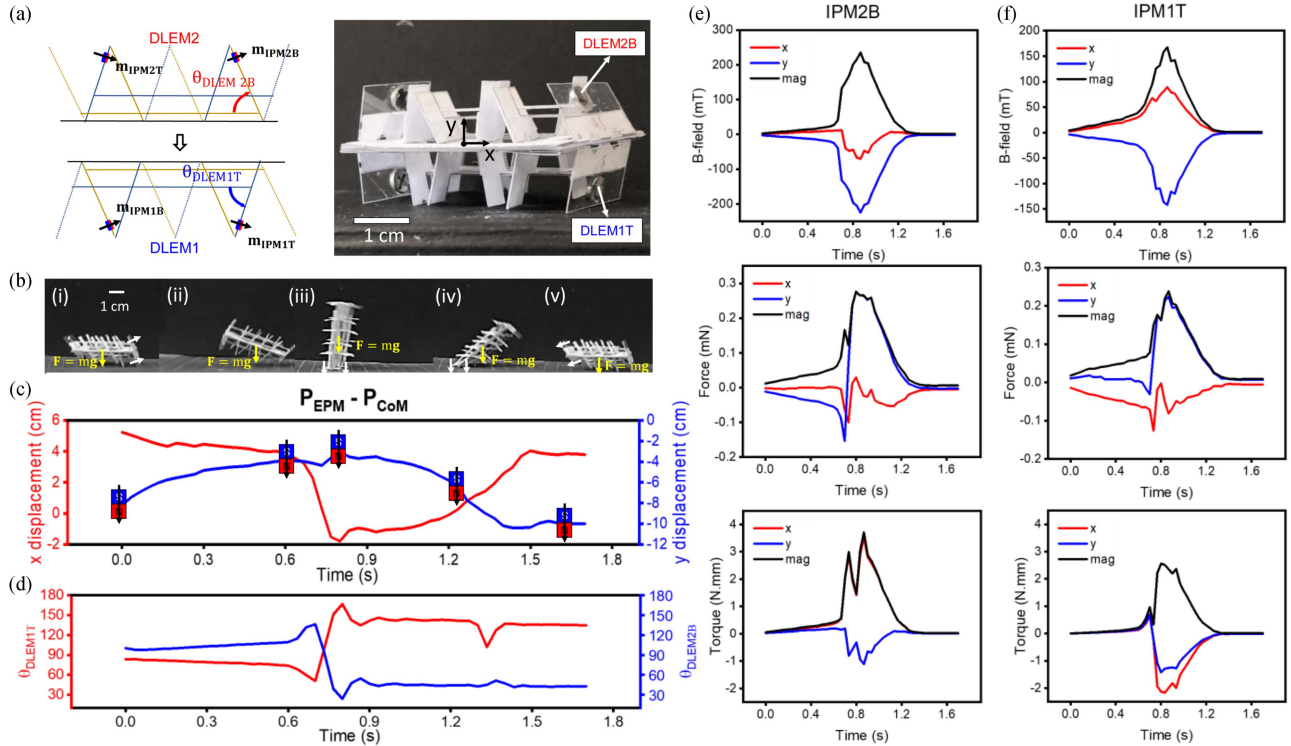CAI et al.: MAGNETICALLY ACTUATED LAMINA EMERGENT MECHANISM FOR BIMODAL CRAWLING AND FLIPPING LOCOMOTION 7

Fig. 4. Magnetic actuation of flipping. (a) Fabrication of an MLEM that can flip by assembling two DLEMs together. (b) Each flipping cycle consists of five phases that can be induced by (c) changing the position and orientation of the EPM along its y-axis. (d) Angle of rotation of the input links of the top and bottom DLEM layer over time. Magnetic flux density, force, and torque exerted on the IPMs on the (e) bottom layer of DLEM2 (IPM2B) and on the (f) top layer of DLEM1 (IPM1T), respectively.

TABLE II
PARAMETER VALUES TO TILT THE MECHANISM

	IPM2B	IPM1T
$|\mathbf{b}|$ (mT)	133	76.0
$|\mathbf{f}|$ (mN)	0.166	0.0780
$|\boldsymbol{\tau}|$ (N·mm)	2.05	0.964

III. RESULTS

The mechanism was actuated on a cutting mat (3 mm thick) to demonstrate crawling and flipping. To track the locomotion performance of the mechanism, a marker was indicated at the CoM of the device, and the original position of the marker was taken to be the origin. We then track the x–y coordinates of the marker overtime during the period of locomotion.

A. Crawling Locomotion

Fig. 5 shows the crawling locomotion performance of the mechanism. In general, the device takes around 23 s to complete the course of 6 cm (∼2.6 mm/s, 0.065 body length/s) when actuated at a frequency of 0.58 Hz [see Fig. 5(a)]. Although the crawling speed of the mechanism in this work is slower than that of our previous work (∼12.4 mm/s, 0.182 body length/s, actuated at 0.6 Hz), our mechanism was able to crawl with more stability without undesirable flipping in the absence of environmental constraints. The basic crawling locomotion mechanism employed by the DLEM is based on friction-inertia motion.

In the case of our mechanism, when the device switches from stance 1 to 2 [(i) and (ii)], as shown in Fig. 5(c), the greater change in the angle of rotation of one LEM layer in contrast to the other will bias the mechanism to move in a direction [see Fig. 5(a)]. Without the difference in the MA between the two LEM linkages, the displacements of the leg tips of the LEMs generated from the rotation cancel each other, leading to little to no net movement. When the device switches back from stance 2 to 1 [(ii) and (iii)], the EPM anchors the mechanism in place, reducing backward slippage. Hence, by switching between the two stances, the mechanism can achieve net forward motion.

Fig. 5(b) shows the angle of rotation of the top and bottom LEM of the bottom DLEM layer. Contrary to what we observed in Fig. 3, the top LEM layer appears to rotate more than the bottom LEM layer, biasing the mechanism to move in the direction of its top LEM layer instead. We observed that, during actuation, the bottom LEM loses contact with the ground due to the greater amount of rotation and is, hence, unable to help push the mechanism forward. To induce the mechanism to move, the EPM is positioned closer to that of the top LEM input linkage than that of the bottom LEM input linkage to reduce the differences in the angle of rotation such that the legs of the bottom LEM layer do not lose contact with the ground. We hypothesize that due to positioning error, the top LEM input linkage may experience greater magnetic force and torque than the bottom LEM and, hence, rotates slightly more.

The speed of the mechanism can be controlled by the frequency of actuation. As observed from Fig. 5(d), by increasing
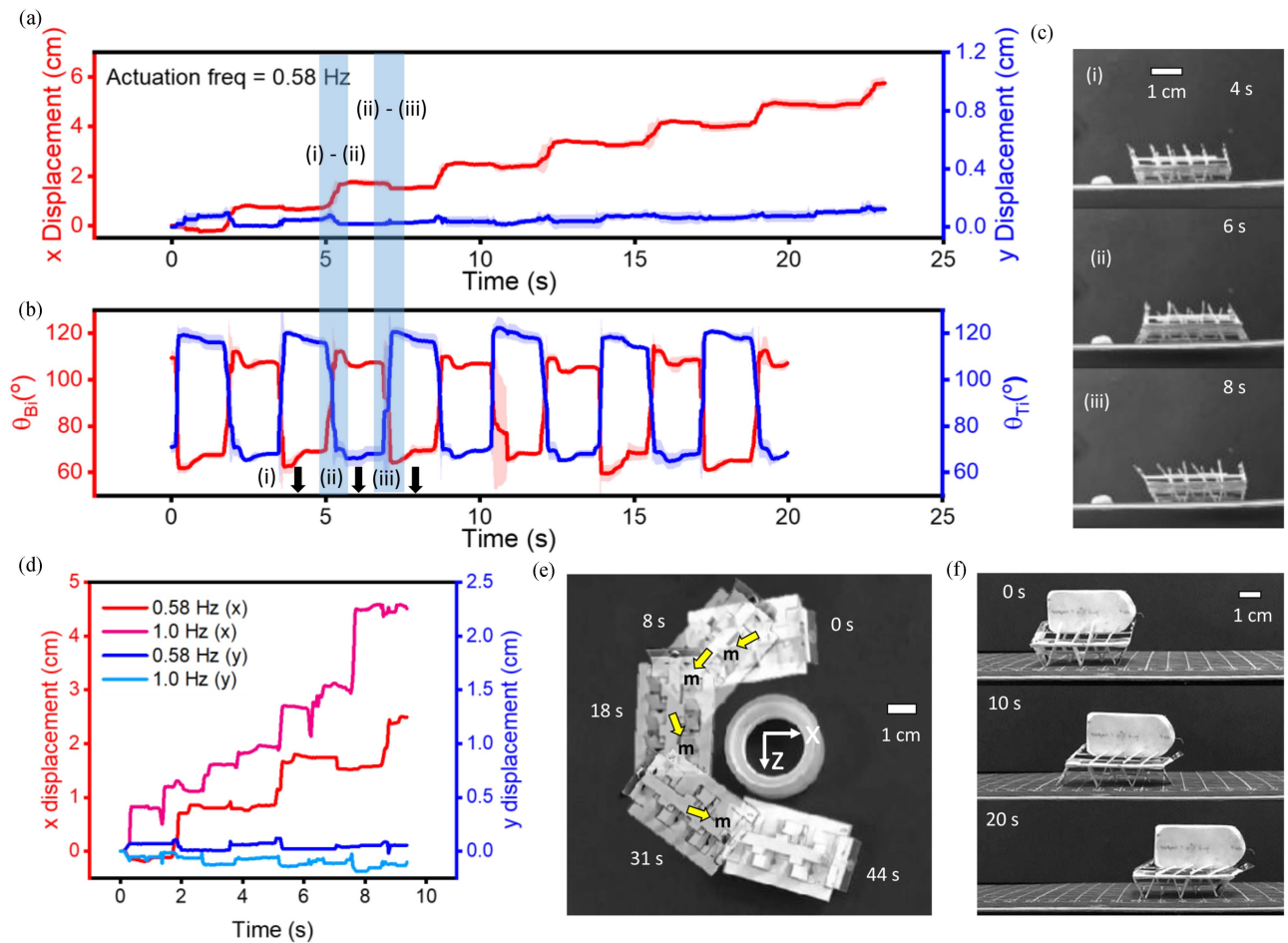
Fig. 5. Crawling performance of the mechanism. (a) x–y displacement of the mechanism over time when actuated at 0.58 Hz. (b) Angle of rotation of the top and bottom LEM linkage of the DLEM contacting the traveling surface. (c) Timestamp of the mechanism switching stances to move. (d) Comparison of the x–y displacement of the mechanism over time when actuated at 1.0 Hz versus at 0.58 Hz. (e) Steering of the mechanism to travel around an object. (f) Mechanism is able to crawl while carrying a load ~576% of its weight.
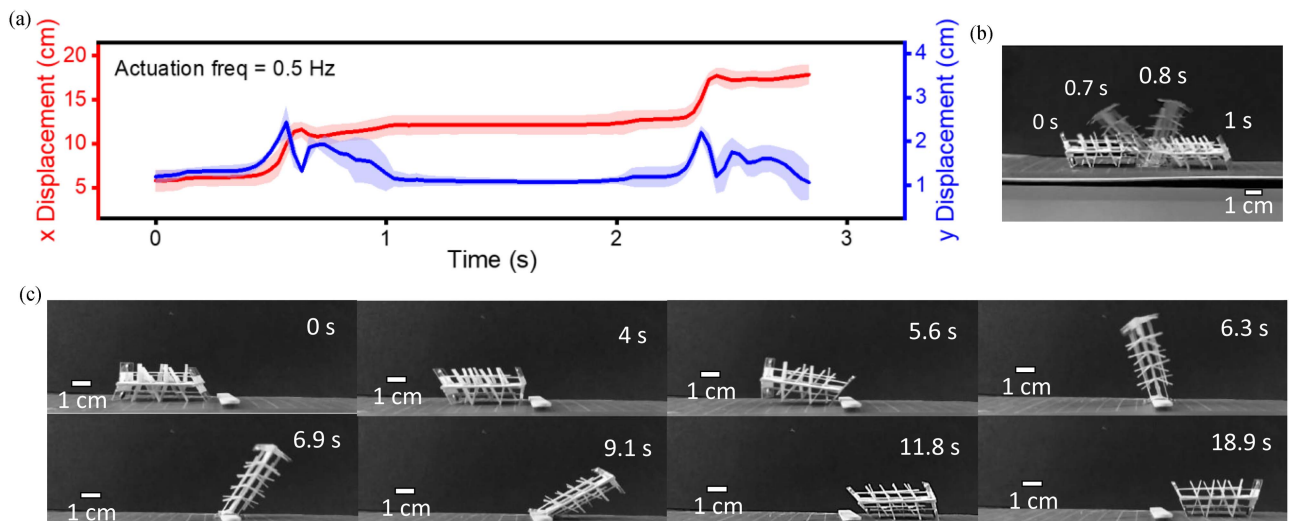

Fig. 6. Flipping performance of the mechanism. (a) x–y displacement of the mechanism over time when actuated at 0.5 Hz. (b) Timestamp of the mechanism undergoing flipping. (c) Using flipping to overcome obstacles (5.6–1.8 s) that cannot be crossed by crawling (0–4 s).

This article has been accepted for inclusion in a future issue of this journal. Content is final as presented, with the exception of pagination.

CAI et al.: MAGNETICALLY ACTUATED LAMINA EMERGENT MECHANISM FOR BIMODAL CRAWLING AND FLIPPING LOCOMOTION 9

the frequency of actuation from 0.58 to 1.0 Hz, the mechanism can achieve a greater speed of $\sim$4.5 mm/s (0.1125 body length/s).

In addition to traveling along a straight line, steering and maneuverable locomotion are crucial. Due to the orientation of the IPMs, the mechanism has a net magnetization along its x-axis. As the net magnetization of the mechanism tends to align with the applied magnetic field, changing the direction of the applied magnetic field in the $x - z$ plane can be used to steer the mechanism via rigid-body rotation. Fig. 5(e) shows how rotating the orientation of the EPM counterclockwise (represented by yellow arrows) can be used to correspondingly rotate the mechanism. By steering the mechanism as it crawls, we demonstrate how it can travel around a circular object.

In addition, to demonstrate the advantages of magnetically actuated compliant mechanisms over their soft counterparts, we actuated the mechanism to crawl under external load. In Fig. 5(f), we showed how the mechanism was able to traverse the planar surface while carrying a load that is $\sim$547% of its body weight.

B. Flipping Locomotion

Fig. 6 shows the locomotion performance of the mechanism flipping two cycles. In general, the device takes around 2.8 s to complete the course of 17.8 cm ($\sim$60.4 mm/s, 1.5 body length/s) when actuated at a frequency of 0.5 Hz [see Fig. 6(a)]. It takes only $\sim$1 s for the robot to flip one cycle [see Fig. 6(b)]. This is significantly faster than the speed attained by the mechanism when crawling, even at twice the actuation frequency.

In terms of terrestrial locomotion, rotational-based locomotion, such as rolling and flipping, is widely used to generate fast on-ground translational motion due to its high speed [11]. In addition, flipping can also be used to overcome obstacles. We demonstrated how flipping could be employed by the mechanism to overcome an obstacle in Fig. 6(c). In contrast to flipping on flat ground, it takes longer for the robot to flip over the obstacle ($\sim$7.8 s). After overcoming the obstacle, the mechanism can continue to crawl or flip.

IV. DISCUSSION

We observe that the relative position and orientation of the EPM primarily influence the type of locomotion generated with respect to the IPMs. By changing the relative positioning and orientation of the EPM with respect to the IPMs, we can achieve the two modes of locomotion.

1) Crawling occurs when the EPM is positioned between the input links of the mechanism, with the magnetization orientation of the EPM aligned along the x-axis.
2) Flipping occurs when the EPM is positioned at the ends of the mechanism, with the magnetization orientation of the EPM aligned along the y-axis.

While flipping can be used to achieve greater locomotion speed and overcome some obstacles, crawling has its advantages in its ability to steer to change directions and avoid larger obstacles. We also observed that, as compared with flipping, the y-displacement of the mechanism does not vary much throughout the crawling actuation cycles, indicating its suitability for more height-limited space. This could potentially be useful in

search and rescue applications or in inspecting and navigating through narrow and collapsed regions [25]. In addition, the slower locomotion speed conferred by crawling makes it more suitable for applications that require slower movements, such as during inspection.

For a preliminary evaluation of the mechanism's locomotion, we manually controlled the position and orientation of the EPM to verify the possibility of using magnetic actuation in generating bimodal locomotion. As a result, the position and orientation of the EPM are not well controlled with respect to the robot. In this work, we estimated the magnetic flux density parameters required to induce and initiate the bimodal locomotion. These values can be used in the control of the mechanism via more controlled systems, such as robotic manipulators and electromagnetic systems.

To better optimize the mechanism, an in-depth understanding of how the differences in MA of the LEMs can be exploited for directional motion is required. Given that friction also plays an important role in the locomotion of the mechanism, it is also important to conduct further characterization of the mechanism on surfaces of various textures and friction coefficients. In addition, the locomotion performance of the mechanism has also yet to be characterized and analyzed on uneven and different terrains, as well as on slopes. Further testing, such as that in our previous works [16], [49], can be carried out as future work. In addition, given that the main advantages of the mechanism lie in the potential for miniaturization, understanding the effects of varying the size of the EPM relative to that of the mechanism can be further explored and verified.

REFERENCES

[1] Z. Yang and L. Zhang, "Magnetic actuation systems for miniature robots: A review," *Adv. Intell. Syst.*, vol. 2, no. 9, 2020, Art. no. 2000082, doi: 10.1002/aisy.202000082.

[2] J. J. Abbott, E. Diller, and A. J. Petruska, "Magnetic methods in robotics," *Annu. Rev. Control, Robot., Auton. Syst.*, vol. 3, no. 1, pp. 57–90, May 2020, doi: 10.1146/annurev-control-081219-082713.

[3] S. Miyashita, S. Guitron, M. Ludersdorfer, C. R. Sung, and D. Rus, "An untethered miniature origami robot that self-folds, walks, swims, and degrades," in *Proc. IEEE Int. Conf. Robot. Autom.*, 2015, pp. 1490–1496, doi: 10.1109/ICRA.2015.7139386.

[4] W. Hu, G. Z. Lum, M. Mastrangeli, and M. Sitti, "Small-scale soft-bodied robot with multimodal locomotion," *Nature*, vol. 554, no. 7690, pp. 81–85, 2018, doi: 10.1038/nature25443.

[5] V. K. Venkiteswaran, D. K. Tan, and S. Misra, "Tandem actuation of legged locomotion and grasping manipulation in soft robots using magnetic fields," *Extreme Mech. Lett.*, vol. 41, 2020, Art. no. 101023.

[6] H. Lu et al., "A bioinspired multilegged soft millirobot that functions in both dry and wet conditions," *Nature Commun.*, vol. 9, no. 1, 2018, Art. no. 3944, doi: 10.1038/s41467-018-06491-9.

[7] C. Laschi, B. Mazzolai, and M. Cianchetti, "Soft robotics: Technologies and systems pushing the boundaries of robot abilities," *Sci. Robot.*, vol. 1, no. 1, 2016, Art. no. eaah3690, doi: 10.1126/scirobotics.aah3690.

[8] Z. Qiji et al., "Soft robotic origami crawler," *Sci. Adv.*, vol. 8, no. 13, Apr. 2022, Art. no. eabm7834, doi: 10.1126/sciadv.abm7834.

[9] A. Chen, R. Yin, L. Cao, C. Yuan, H. K. Ding, and W. J. Zhang, "Soft Robotics: Definition and research issues," in *Proc. 24th Int. Conf. Mechatronics Mach. Vis. Pract.*, 2017, pp. 366–370.

[10] S. Miyashita, S. Guitron, K. Yoshida, S. Li, D. D. Damian, and D. Rus, "Ingestible, controllable, and degradable origami robot for patching stomach wounds," in *Proc. IEEE Int. Conf. Robot. Autom.*, 2016, pp. 909–916, doi: 10.1109/ICRA.2016.7487222.

[11] Q. Ze et al., "Spinning-enabled wireless amphibious origami millirobot," *Nature Commun.*, vol. 13, no. 1, 2022, Art. no. 3118, doi: 10.1038/s41467-022-30802-w.

This article has been accepted for inclusion in a future issue of this journal. Content is final as presented, with the exception of pagination.

10   IEEE/ASME TRANSACTIONS ON MECHATRONICS

[12] S. Miyashita, S. Guitron, S. Li, and D. Rus, "Robotic metamorphosis by origami exoskeletons," *Sci. Robot.*, vol. 2, no. 10, 2017, Art. no. eaao4369, doi: 10.1126/scirobotics.aao4369.

[13] B. S. Yeow et al., "Magnetically steerable serial and parallel structures by mold-free origami templating and domain setting," *Adv. Mater. Technol.*, vol. 7, no. 6, 2022, Art. no. 2101140.

[14] D. Rus and M. T. Tolley, "Design, fabrication and control of origami robots," *Nature Rev. Mater.*, vol. 3, no. 6, pp. 101–112, 2018, doi: 10.1038/s41578-018-0009-8.

[15] J. O. Jacobsen, B. G. Winder, L. L. Howell, and S. P. Magleby, "Lamina emergent mechanisms and their basic elements," *J. Mechanisms Robot.*, vol. 2, no. 1, 2010, Art. no. 011003, doi: 10.1115/1.4000523.

[16] T. N. L. Giang, C. J. Cai, G. Ponraj, and H. Ren, "Magnetically deployable robots using layered lamina emergent mechanism," *Appl. Sci.*, vol. 12, no. 1, 2022, Art. no. 14, doi: 10.3390/app12010014.

[17] P. S. Gollnick, S. P. Magleby, and L. L. Howell, "An introduction to multilayer lamina emergent mechanisms," *J. Mech. Des.*, vol. 133, no. 8, 2011, Art. no. 081006, doi: 10.1115/1.4004542.

[18] X. Hao et al., "Analysis of spiders' joint kinematics and driving modes under different ground conditions," *Appl. Bionics Biomech.*, vol. 2019, 2019, Art. no. 4617212, doi: 10.1155/2019/4617212.

[19] W. Neubauer, "A spider-like robot that climbs vertically in ducts or pipes," in *Proc. IEEE/RSJ Int. Conf. Intell. Robots Syst.*, 1994, pp. 1178–1185.

[20] Z. Wang, J. Wang, A. Ji, H. Li, and Z. Dai, "Movement behavior of a spider on a horizontal surface," *Chin. Sci. Bull.*, vol. 56, no. 25, pp. 2748–2757, 2011, doi: 10.1007/s11434-011-4584-y.

[21] H. C. Greenberg, "The application of origami to the design of lamina emergent mechanisms (LEMs) with extensions to collapsible, compliant and flat-folding mechanisms," M.S. thesis, Dept. Mech. Eng., Brigham Young Univ., Provo, UT, USA, 2012.

[22] G. Rothenhofer, C. Walsh, and A. Slocum, "Transmission ratio based analysis and robust design of mechanisms," *Precis. Eng.*, vol. 34, no. 4, pp. 790–797, 2010, doi: 10.1016/j.precisioneng.2010.03.010.

[23] B. G. Winder, S. P. Magleby, and L. L. Howell, "Kinematic representations of pop-up paper mechanisms," *J. Mechanisms Robot.*, vol. 1, no. 2, 2009, Art. no. 021009, doi: 10.1115/1.3046128.

[24] C. D. Onal, R. J. Wood, and D. Rus, "An origami-inspired approach to worm robots," *IEEE/ASME Trans. Mechatron.*, vol. 18, no. 2, pp. 430–438, Apr. 2013, doi: 10.1109/TMECH.2012.2210239.

[25] M. Yu, W. Yang, Y. Yu, X. Cheng, and Z. Jiao, "A crawling soft robot driven by pneumatic foldable actuators based on Miura-Ori," *Actuators*, vol. 9, no. 2, 2020, Art. no. 26.

[26] N. B. Albrechtsen, S. P. Magleby, and L. L. Howell, "Identifying potential applications for lamina emergent mechanisms using technology push product development," in *Proc. Int. Des. Eng. Tech. Conf. Comput. Inf. Eng. Conf.*, 2010, pp. 513–521.

[27] J. Mu, C. Hou, H. Wang, Y. Li, Q. Zhang, and M. Zhu, "Origami-inspired active graphene-based paper for programmable instant self-folding walking devices," *Sci. Adv.*, vol. 1, no. 10, 2015, Art. no. e1500533, doi: 10.1126/sciadv.1500533.

[28] H. Yang et al., "Multifunctional metallic backbones for origami robotics with strain sensing and wireless communication capabilities," *Sci. Robot.*, vol. 4, no. 33, 2019, Art. no. eaax7020.

[29] S. Sundaram, D. S. Kim, M. A. Baldo, R. C. Hayward, and W. Matusik, "3D-printed self-folding electronics," *ACS Appl. Mater. Interfaces*, vol. 9, no. 37, pp. 32290–32298, 2017, doi: 10.1021/acsami.7b10443.

[30] Y. Liu, B. Shaw, M. D. Dickey, and J. Genzer, "Sequential self-folding of polymer sheets," *Sci. Adv.*, vol. 3, no. 3, 2017, Art. no. e1602417, doi: 10.1126/sciadv.1602417.

[31] H. Suzuki and R. J. Wood, "Origami-inspired miniature manipulator for teleoperated microsurgery," *Nature Mach. Intell.*, vol. 2, pp. 437–446, 2020.

[32] W. Yue et al., "Origami-inspired structure with pneumatic-induced variable stiffness for multi-DOF force-sensing," *Sensors*, vol. 22, no. 14, 2022, Art. no. 5370.

[33] T. Amadeo et al., "Soft robotic deployable origami actuators for neurosurgical brain retraction," *Front. Robot. AI*, vol. 8, no. 1, 2022, Art. no. 731010, doi: 10.3389/frobt.2021.731010.

[34] D. Brown and A. J. Cox, "Innovative uses of video analysis," *Phys. Teacher*, vol. 47, no. 3, pp. 145–150, 2009.

[35] A. W. Mahoney and J. J. Abbott, "Five-degree-of-freedom manipulation of an untethered magnetic device in fluid using a single permanent magnet with application in stomach capsule endoscopy," *Int. J. Robot. Res.*, vol. 35, no. 1/3, pp. 129–147, 2016.

[36] P. Ryan and E. Diller, "Magnetic actuation for full dexterity microrobotic control using rotating permanent magnets," *IEEE Trans. Robot.*, vol. 33, no. 6, pp. 1398–1409, Dec. 2017, doi: 10.1109/TRO.2017.2719687.

[37] A. W. Mahoney, D. L. Cowan, K. M. Miller, and J. J. Abbott, "Control of untethered magnetically actuated tools using a rotating permanent magnet in any position," in *Proc. IEEE Int. Conf. Robot. Autom.*, 2012, pp. 3375–3380.

[38] L. Sliker, G. Ciuti, M. Rentschler, and A. Menciassi, "Magnetically driven medical devices: A review," *Expert Rev. Med. Devices*, vol. 12, no. 6, pp. 737–752, 2015, doi: 10.1586/17434440.2015.1080120.

[39] J. D. Black, "Evaluation and development of actuators for lamina emergent mechanisms with emphasis on flat solenoids," M.Sc. thesis, Dept. Mech. Eng., Brigham Young Univ., Provo, UT, USA, 2012.

[40] K. B. Baltzis, "The finite element method magnetics (FEMM) freeware package: May it serve as an educational tool in teaching electromagnetics," *Educ. Inf. Technol.*, vol. 15, no. 1, pp. 19–36, 2010, doi: 10.1007/s10639-008-9082-8.

[41] P. A. Bogdan, J. Wheadon, F. B. Klein, and M. Gianni, "Magnetic tracked robot for internal pipe inspection," in *Proc. Eur. Conf. Mobile Robots*, 2021, pp. 1–6, doi: 10.1109/ECMR50962.2021.9568790.

[42] M. Duduta, F. Berlinger, R. Nagpal, D. R. Clarke, R. J. Wood, and F. Z. Temel, "Tunable multi-modal locomotion in soft dielectric elastomer robots," *IEEE Robot. Autom. Lett.*, vol. 5, no. 3, pp. 3868–3875, Jul. 2020, doi: 10.1109/LRA.2020.2983705.

[43] C. Dunning, R. Cervantes, L. Velasquez, A. Western, M. Sherman, and M. Hassanalian, "Design and manufacturing of a bioinspired spider rolling robot for Mars exploration," in *Proc. AIAA Scitech 2021 Forum*, 2021, Paper 958.

[44] T. Yanagida, R. E. Mohan, T. Pathmakumar, K. Elangovan, and M. Iwase, "Design and implementation of a shape shifting rolling–crawling–wall-climbing robot," *Appl. Sci.*, vol. 7, no. 4, 2017, Art. no. 342, doi: 10.3390/app7040342.

[45] R. D. Shi, X. L. Zhang, and Y. A. Yao, "A CPG-based control method for the multi-mode locomotion of a desert spider robot," *Robot*, vol. 40, no. 2, pp. 146–157, 2018, doi: 10.13973/j.cnki.robot.170294.

[46] N. Tan, R. E. Mohan, and K. Elangovan, "Scorpio: A biomimetic reconfigurable rolling-crawling robot," *Int. J. Adv. Robot. Syst.*, vol. 13, no. 5, pp. 1–16, 2016, doi: 10.1177/1729881416658180.

[47] N. Tan, R. E. Mohan, and K. Elangovan, "A bio-inspired reconfigurable robot," in *Advances in Reconfigurable Mechanisms and Robots II*, X. Ding, X. Kong, and J. S. Dai, Eds. Berlin, Germany: Springer, 2016, pp. 483–493.

[48] Z. Zhakypov, K. Mori, K. Hosoda, and J. Paik, "Designing minimal and scalable insect-inspired multi-locomotion millirobots," *Nature*, vol. 571, no. 7765, pp. 381–386, 2019, doi: 10.1038/s41586-019-1388-8.

[49] C. J. Cai et al., "Diversified and untethered motion generation via crease patterning from magnetically actuated caterpillar-inspired origami robot," *IEEE/ASME Trans. Mechatron.*, vol. 26, no. 3, pp. 1678–1688, Jun. 2021.

Catherine Jiayi Cai received the B.Eng. degree in biomedical engineering from the National University of Singapore, Singapore, in 2019. She is currently working toward the Ph.D. degree in biomedical engineering with Medical Mechatronics Group, National University of Singapore, Singapore, and the Singapore Institute of Manufacturing Technology, Agency for Science, Technology and Research, Singapore.

Bok Seng Yeow (Graduate Student Member, IEEE) received the B.Eng. degree in biomedical engineering in 2016 from the National University of Singapore, Singapore, where he is currently working toward the Ph.D. degree in biomedical engineering with Medical Mechatronics Group.

This article has been accepted for inclusion in a future issue of this journal. Content is final as presented, with the exception of pagination.

CAI et al.: MAGNETICALLY ACTUATED LAMINA EMERGENT MECHANISM FOR BIMODAL CRAWLING AND FLIPPING LOCOMOTION   11

Hui Huang received the Ph.D. degree in micro-electronics from Xi'an Jiaotong University, Xi'an, China, in 2004.

He is a Scientist with the Singapore Institute of Manufacturing Technology (SIMTech), Agency for Science, Technology and Research, Singapore. His research areas include nanomaterials, functional coatings and devices with particular emphasis on printed electronics, energy efficiency, energy conversion, and storage. Prior to joining SIMTech, he was a Lee Kuan Yew Postdoctoral Fellow with the School of Electrical and Electronic Engineering, Nanyang Technological University.

Dr. Huang was a recipient of the Singapore Millennium Foundation Scholar in 2008.

Cecilia Laschi (Fellow, IEEE) received the Graduate degree in computer science from the University of Pisa, Pisa, Italy, in 1993, and the Ph.D. degree in robotics from the University of Genoa, Genoa, Italy, in 1998.

She is a Professor with the Department of Mechanical Engineering, National University of Singapore, Singapore. She was a JSPS Visiting Researcher with Waseda University, Tokyo, Japan, in 2001 and 2002. She is an Editor-in-Chief for *Bioinspiration and Biomimetics* and a member of the Editorial Boards of a few journals, including *Science Robotics*. She serves as a reviewer for journals, such as *Nature* and *Science*, for EC (including the ERC program), HFSP, and national research agencies. She cofounded the spin-off ROBOTECH S.r.l, Pisa, Italy. Her research interests include soft robotics, an area she pioneered and contributed to develop internationally, including its marine and biomedical applications. She has been working in humanoid and neurorobotics. She authored or coauthored more than 300 scientific papers.

Dr. Laschi is a Senior Member of EMBS and RAS, where she is also an AdCom member and founding Co-Chair of the TC on Soft Robotics. She founded and chaired the 1st IEEE-RAS International Conference on Soft Robotics.

Hongliang Ren (Senior Member, IEEE) received the Ph.D. degree in electronic engineering (specialized in biomedical engineering) from The Chinese University of Hong Kong, Hong Kong, in 2008.

He has served as an Associate Editor for IEEE TRANSACTIONS ON AUTOMATION SCIENCE AND ENGINEERING and *Medical and Biological Engineering and Computing*. He has navigated his academic journey through the Chinese University of Hong Kong, Johns Hopkins University, Children's Hospital Boston, Harvard Medical School, Children's National Medical Center, United States, and National University of Singapore. His areas of interest include biorobotics, intelligent control, medical mechatronics, soft continuum robots, soft sensors, and multisensory learning in medical robotics.

Dr. Ren was the recipient of the NUS Young Investigator Award and Engineering Young Researcher Award 2018, IAMBE Early Career Award 2018, Interstellar Early Career Investigator Award 2018, and ICBHI Young Investigator Award 2019.